Supplementary information

Lattice dynamics of the Zn-Mg-Sc icosahedral quasicrystal and its Zn-Sc periodic 1/1 approximant.

Marc de Boissieu[1][**], Sonia Francoual [1,2][*], Marek Mihalkovič[3,1], Kaoru Shibata[4], , Alfred Q.R. Baron[5,6], Yvan Sidis[7], Tsutomu Ishimasa[8], Dongmei Wu[9], Thomas Lograsso[9], Louis-Pierre Regnault[10], Franz Gähler [11], Satoshi Tsutsui[6], Bernard Hennion[7], Pierre Bastie[12,2], Taku J. Sato[13], Hiroyuki Takakura[8], Roland Currat[2], An-Pang Tsai[14]

1- Pseudo Brillouin zones

The concept of pseudo Brillouin zone boundary (PBZB) can be derived within a weak coupling type theory[1-3]. Within this framework one can show that the acoustic dispersion curve should display a gap opening at pseudo Brillouin zone boundaries (PBZB), whose position in reciprocal space is defined by $q_{PBZB} = Q_{Bragg}/2$, where Q_{Bragg} is a reciprocal lattice vector of the quasicrystal. Although the reciprocal space is densely filled in a QC, only the strongest Fourier components are relevant, the width of the gap being proportional to the amplitude of the structure factor $F(Q_{Bragg})$.

To select the main zone boundaries we have considered the measured X-ray structure factors. Unlike the case of electron, where the important Bragg planes are those with a length close to the Fermi sphere radius, in the case of phonon one has to consider rather small Q_{Bragg} wavevectors in the range 0 to 2 $\mathring{A}^{-1}$, or q_{PBZB} in the range 0 to 1 $\mathring{A}^{-1}$, since the acoustic regime only holds for q smaller than 0.6 $\mathring{A}^{-1}$. These PBZB are placed around the strong Bragg peaks acting as zone centres [4,5] and are displayed as vertical dashed line in the figures. This approximation is only valid in the vicinity of the zone centre, where the acoustic mode is well defined.

When compared with the distribution of Brillouin zone in the 1/1 approximant, it can be shown that the first BZB of the 1/1 approximant, located at 0.45 $\mathring{A}^{-1}$, is replaced by two consecutives PBZB located at 0.33 $\mathring{A}^{-1}$ and 0.53 $\mathring{A}^{-1}$ associated with the 4/0 and 4/4 2-fold axis reflections, as shown by the vertical lines in Figure 2. Indeed, when applying the appropriate phason strain transformation those two reflections transforms into the (2 0 0) reflection in the approximant. Moreover when comparing the structure factors of the two QC reflections to that of the approximant's single reflection one finds that their respective intensities are smaller (0.008 and 0.017 to be compared to 0.035). As a result one expects thus a weaker Bragg plane reflection in the QC than in the approximant.

2- Modelling.

As explained in the text a crucial parameter in modelling the 1/1 approximant and the QC is the orientational disorder of the tetrahedra. In the 1/1 approximant supercell model, the 8 tetrahedra orientations are chosen randomly (12 possibilities for each). Room-T molecular dynamic annealing is then performed and followed by a quench at 0K where accurate relaxation is carried out. The same procedure was used for the QC. The S(Q,E) response function is then calculated with the quench model. This ensures that the proper weak correlations between tetrahedra are taken into account, inducing broadening and mode mixing in the response function. On the contrary simulations made on a 2 clusters 1/1 model (i.e.

without a supercell and no tetrahedral disorder), leads to a much more structured spectral function, as shown Figure S2.

The figure S1, displays the diffraction pattern of the simulated 1/1 and 3/2 approximant.
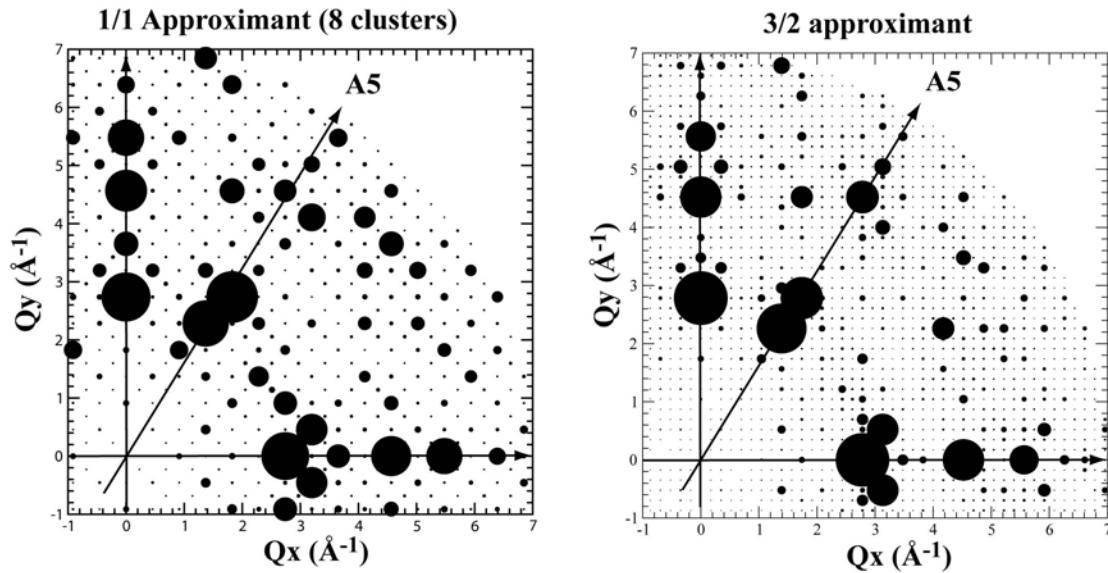

Figure S1:

Simulated diffracted patterns. The left panel displays the diffraction pattern for the super-cell 1/1 approximant containing 8 clusters per unit cell, once quenched to 0K. The right panel displays the diffraction pattern of the 3/2 approximant. The area of the dots is proportional to the Bragg peak intensity and is scaled so as to be compared directly with the experimental data Figure 1. Although the 3/2 approximant clearly shows lattice periodicity, the intensity distribution of the strongest Bragg peaks matches well the one of the quasicrystal in Figure1 c.
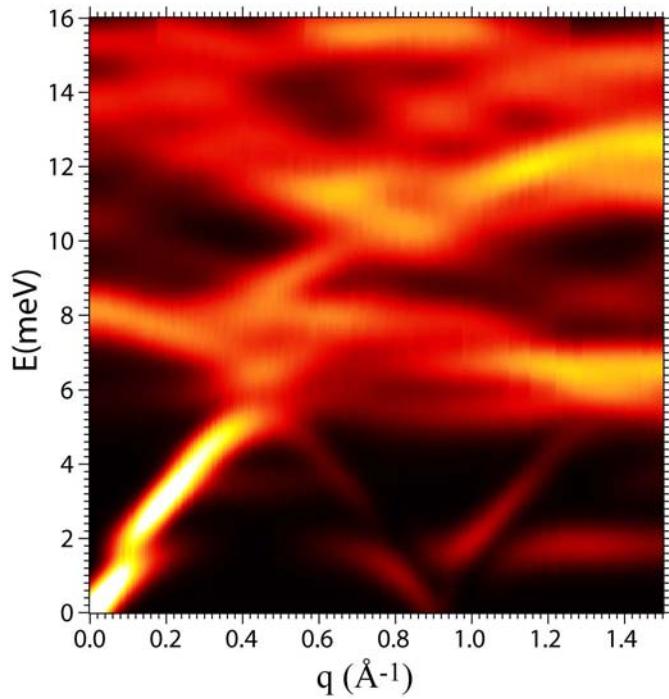
Figure S2:

Simulated S(**Q**,E) response function for an 1/1 model having Im3 symmetry. The scattering geometry is transverse and the same as Figure 4. In this model the inner tetrahedra are oriented in such a way that they fulfill the Im3 symmetry constraint. This should be compared to Figure 4, left panel, where the super-cell model has been used. The Im3 symmetry model displays features which are neither seen experimentally, nor in the simulation using the super-cell model. In particular gaps are showing up at low energy (here around 1.6 meV). Moreover, the optical-like excitations are much more structured. Indeed, the introduction of the random orientation of the tetrahedron smoothes out the overall intensity distribution of the S(**Q**,E) response function for optical excitations.

References

1.   Smith, A. P. & Ashcroft, N. W. Pseudopotentials and quasicrystals. *Phys. Rev. Lett.* **59(12)**, 1365-1368 (1987).
2.   Lu, J. P. & Birman, J. Acoustic-wave propagation in quasiperiodic, incommensurate, and random systems. *Phys. Rev. B* **38(12)**, 8067-8074 (1988).
3.   Quilichini, M. & Janssen, T. Phonons in quasicrystals. *Rev. Mod. Phys.* **69**, 277 (1997).
4.   Niizeki, K. & Akamuatsu, T. The reciprocal space properties of the electronic wave functions of the Penrose lattice. *Journal of Physics: Condensed Matter* **2(33)**, 7043-7047 (1990).
5.   Niizeki, K. & Akamatsu, T. Special points in the reciprocal space of an icosahedral quasi-crystal and the quasi-dispersion relation of electrons. *J. Phys: Cond. Matter* **2(12)**, 2759-2771 (1990).